Cellular/Molecular

Synaptic Contributions to Cochlear Outer Hair Cell Ca^{2+} Dynamics

Marcelo J. Moglie, Diego L. Wengier, A. Belén Elgoyhen, and Juan D. Goutman
Instituto de Investigaciones en Ingeniería Genética y Biología Molecular "Dr. Héctor N. Torres" (INGEBI) (Consejo Nacional de Investigaciones Científicas y Tecnológicas), Ciudad Autónoma de Buenos Aires 1428, Argentina

For normal cochlear function, outer hair cells (OHCs) require a precise control of intracellular Ca^{2+} levels. In the absence of regulatory elements such as proteinaceous buffers or extrusion pumps, OHCs degenerate, leading to profound hearing impairment. Influx of Ca^{2+} occurs both at the stereocilia tips and the basolateral membrane. In this latter compartment, two different origins for Ca^{2+} influx have been poorly explored: voltage-gated L-type Ca^{2+} channels (VGCCs) at synapses with Type II afferent neurons, and α9α10 cholinergic nicotinic receptors at synapses with medio-olivochlear complex (MOC) neurons. Using functional imaging in mouse OHCs, we dissected Ca^{2+} influx individually through each of these sources, either by applying step depolarizations to activate VGCC, or stimulating MOC axons. Ca^{2+} ions originated in MOC synapses, but not by VGCC activation, was confined by Ca^{2+}-ATPases most likely present in nearby synaptic cisterns. Although Ca^{2+} currents in OHCs are small, VGCC Ca^{2+} signals were comparable in size to those elicited by α9α10 receptors, and were potentiated by ryanodine receptors (RyRs). In contrast, no evidence of potentiation by RyRs was found for MOC Ca^{2+} signals over a wide range of presynaptic stimulation strengths. Our study shows that despite the fact that these two Ca^{2+} entry sites are closely positioned, they differ in their regulation by intracellular cisterns and/or organelles, suggesting the existence of well-tuned mechanisms to separate the two different OHC synaptic functions.

Key words: **α9α10; calcium; cistern; outer hair cell; synapses; voltage-gated Ca^{2+} channels**

Significance Statement

Outer hair cells (OHCs) are sensory cells in the inner ear operating under very special constraints. Acoustic stimulation leads to fast changes both in membrane potential and in the intracellular concentration of metabolites such as Ca^{2+}. Tight mechanisms for Ca^{2+} control in OHCs have been reported. Interestingly, Ca^{2+} is crucial for two important synaptic processes: inhibition by efferent cholinergic neurons, and glutamate release onto Type II afferent fibers. In the current study we functionally imaged Ca^{2+} at these two different synapses, showing close positioning within the basolateral compartment of OHCs. In addition, we show differential regulation of these two Ca^{2+} sources by synaptic cisterns and/or organelles, which could result crucial for functional segregation during normal hearing.

Introduction

Efficient compartmentalization of Ca^{2+} signaling is crucial for normal cell function and to enhance the computational power of individual cells (Bootman et al., 2001; Petersen, 2002; Augustine et al., 2003). However, if not tightly controlled spatially and temporally within cells, it could generate severe cell dysfunction and even cell death (Choi, 1995). Cochlear outer hair cells (OHCs) are a unique group of cells responsible for sound amplification within the inner ear that present a highly polarized structure, featuring a stereocilia bundle on their apical end and synaptic connections on the basolateral membrane (Fuchs, 1996; Dallos, 2008; Fettiplace, 2017). One important aspect of OHC physiology is the precise homeostasis and tight regulation of Ca^{2+} during normal activity. The main Ca^{2+} source are mechanotransducer channels located at the tip of stereocilia (Beurg et al., 2009; Fettiplace and Nam, 2019). Within OHCs stereocilia high concentrations of proteinaceous Ca^{2+} buffers coexist with large amounts of extrusion pumps, suggesting the need for quick clearing mechanisms (Sakaguchi et al., 1998; Yamoah et al., 1998; Dumont et al., 2001; Hackney et al., 2005; Chen et al., 2012). Deficits in these control pathways, because of mutations in Ca^{2+}-ATPases or the absence of the Ca^{2+} buffer oncomodulin, lead to OHCs loss and

Received Nov. 29, 2020; revised May 30, 2021; accepted July 5, 2021.

Author contributions: M.J.M., A.B.E., and J.D.G. designed research; M.J.M. and D.L.W. performed research; M.J.M. and J.D.G. analyzed data; M.J.M., D.L.W., A.B.E., and J.D.G. edited the paper; J.D.G. wrote the first draft of the paper; J.D.G. wrote the paper.

This work was supported by the Agencia Nacional de Promoción Científica y Tecnológica Grant PICT 2016-2155 (to J.D.G.) and the National Institutes of Health Grant R01 DC001508 (to P.A.F. and A.B.E.). We thank Maryline Beurg for advice on the use of ascorbic acid in the intracellular solution and Joe Santos-Sacchi on OHCs recordings, J. Dempster for the use of WinWCP, and Paul A. Fuchs for comments on the manuscript.

The authors declare no competing financial interests.

Correspondence should be addressed to Juan D. Goutman at goutman@dna.uba.ar.

https://doi.org/10.1523/JNEUROSCI.3008-20.2021

Copyright © 2021 the authors

profound auditory deficits (Street et al., 1998; Ficarella et al., 2007; Tong et al., 2016).

Two other important Ca^{2+} sources in OHCs have been less characterized: the voltage-gated L-type Ca^{2+} channels (VGCC; Knirsch et al., 2007), and the $\alpha9\alpha10$ cholinergic nicotinic receptors (Weisstaub et al., 2002; Gómez-Casati et al., 2005). Both VGCC and $\alpha9\alpha10$ receptors are located at the basolateral membrane of OHCs, at synapses with Type II afferent fibers in the case of the former (Saito, 1990), and on the postsynaptic side of synapses with medio-olivochlear complex (MOC) fibers in the latter (Elgoyhen et al., 1994, 2001). Compared with inner hair cells (IHCs), OHCs show smaller Ca^{2+} currents through VGCC (Knirsch et al., 2007; Beurg et al., 2008; Johnson and Marcotti, 2008; Wong et al., 2013), and present synaptic ribbons with irregular shapes and fewer vesicles in their vicinity (for review, see Fuchs and Glowatzki, 2015). These synapses are weak as they only release few vesicles on stimulation contrasting with the multivesicular exocytosis at IHCs afferent synapses (Glowatzki and Fuchs, 2002; Weisz et al., 2009; Fuchs and Glowatzki, 2015). It has been suggested that Type II fibers would only be activated in loud environments, and possibly be responsible for signaling pain in the inner ear (Flores et al., 2015; Liu et al., 2015; Weisz et al., 2021).

On the other hand, cholinergic MOC synapses onto OHCs are inhibitory and provide the means to modulate sound amplification (Guinan, 1996). Synaptic responses are mediated by the highly Ca^{2+}-permeable $\alpha9\alpha10$ receptors, coupled to the activation of SK2 (Ca^{2+}-activated K^+) channels leading to OHCs hyperpolarization (Fuchs, 1996; Weisstaub et al., 2002; Gómez-Casati et al., 2005). Detailed electron micrographs have shown postsynaptic cisterns within OHCs, closely aligned with presynaptic efferent synaptic contacts (Engström, 1958; Smith and Sjöstrand, 1961; Saito, 1980; Fuchs et al., 2014). In analogy to the sarcoplasmic reticulum found in myocytes, synaptic cisterns have been proposed to serve as Ca^{2+} stores that modulates efferent synaptic responses through both Ca^{2+} ATPases (of the sarcoplasmic type, SERCA) responsible for pumping Ca^{2+} ions out of the cytoplasm and into the cistern; and ryanodine receptors (RyRs), which trigger the phenomenon of Ca^{2+}-induced Ca^{2+} release (CICR; Evans et al., 2000; Grant et al., 2006; Lioudyno et al., 2004; Sridhar et al., 1997). The functional evidence to support these observations is indirect, but the presence of SERCA in synaptic cisterns, and RyR in both synaptic and lateral wall cisterns has been documented before (Lioudyno et al., 2004; Grant et al., 2006).

In the present work, we performed functional Ca^{2+} imaging studies to dissect OHCs Ca^{2+} dynamics at their basolateral compartment. Using an *ex vivo* preparation of the cochlea from post-hearing onset mice, we found that Ca^{2+} signals from VGCC are much smaller than those observed in IHCs (Wong et al., 2013; Moglie et al., 2018) but comparable in amplitude to those through $\alpha9\alpha10$ receptors. Moreover, they can be potentiated by RyR. On the contrary, Ca^{2+} transients produced by $\alpha9\alpha10$ activation were not affected by RyR, and were efficiently confined by cisternal Ca^{2+}-ATPases. Thus, the present results indicate that these two Ca^{2+} sources in OHCs present different regulation mechanisms, despite a very close physical proximity.

Materials and Methods

Electrophysiological recordings from OHCs

Euthanasia and tissue extraction were conducted according to approved animal protocols of INGEBI Institutional Animal Care and Use Committee. Excised apical turns of 12- to 14-d-old mouse cochleas (BALB/c, either sex) were placed into a chamber on the stage of an upright microscope (Olympus BX51WI) and used within 2 h. OHCs were visualized on a monitor via a water immersion objective (60×), difference interference contrast optics and a CCD camera (Andor iXon 885). All recordings were performed at room temperature (22–25°C). Because of the short viability of the cochlear preparation and OHCs at this age, only one cell could be recorded per animal.

The cochlear preparation was superfused continuously at 2–3 ml/min with extracellular saline solution of an ionic composition similar to that of the perilymph: 144 mM NaCl, 5.8 mM KCl, 1.3 mM $CaCl_2$, 0.7 mM NaH_2PO_4, 5.6 mM D-glucose, 10 mM HEPES buffer, 2 mM pyruvate, and 3 mM myo-inositol, pH 7.4. Working solutions containing different drugs were made up in this same saline and delivered through the perfusion system. Recording pipettes were fabricated from 1 mm borosilicate glass (WPI), with tip resistances of 6–8 MΩ. Series resistance errors were not compensated for.

For all experiments, the basic pipette solution was made from a 1.25× stock to reach a final concentration of 95 mM KCl, 40 mM K-ascorbate, 5 mM HEPES, 2 mM pyruvate, 6 mM $MgCl_2$, 5 mM Na_2ATP, 10 mM phosphocreatine-Na_2, 0.5 mM EGTA, and 0.4 mM Ca^{2+} indicator (Fluo-4), pH 7.2. To avoid variations in OHCs volume during experiments, pressure in the recording system was controlled with a digital manometer and kept within 5- to 9-cm H_2O range.

Efferent synaptic currents were evoked by unipolar electrical stimulation of the MOC efferent axons as described previously (Goutman et al., 2005; Ballestero et al., 2011). Briefly, the electrical stimulus was delivered via a 20- to 80-µm-diameter glass pipette which position was adjusted until postsynaptic currents in OHCs were consistently activated. An electrically isolated constant current source (model DS3, Digitimer) was triggered via the data-acquisition computer to generate pulses of 40–220 µA, 1-ms width. Further increasing stimulation intensity, or duration, did not produce any rise in release probability (or reduction in failure rate). Solutions containing acetylcholine (ACh) were applied by a gravity-fed multichannel glass pipette (150-µm tip diameter).

Electrophysiological recordings were performed using a Multiclamp 700B amplifier (Molecular Devices), low-pass filtered at 6 kHz and digitized at 50 kHz via a National Instruments board. Data were acquired using WinWCP (J. Dempster, University of Strathclyde). To maximize Ca^{2+} driving force during imaging experiments, OHCs were voltage clamped at −100 mV, but only during a brief period of time when stimulation was applied and synaptic responses were recorded (650 ms in paired pulse experiments, and 2 s in trains). Otherwise, cells were held at −40 mV. Electric shocks to MOC fibers were separated by intervals of 5 s in paired pulse experiments, and 30 s for trains. Recordings were analyzed with custom-written routines in IgorPro 6.37 (Wavemetrics). IPSCs were evaluated as successfully activated when met a double criteria: (1) the amplitude of the current right after the stimulation artifact was >3× SD of the basal current; and (2) the integral of the IPSC was >0.3 pC, which is the average integral of a single synaptic event (Ballestero et al., 2011).

Chemicals

Stock solutions of dantrolene, thapsigargin, and ryanodine (both at 1 and 100 µM) were prepared in DMSO and added to the intracellular solution, such that the concentration of DMSO in the pipette solution was 0.5% v/v in every case. All salts and drugs were acquired from Sigma except for ryanodine, dantrolene and thapsigargin which were purchased from Tocris.

Ca^{2+} imaging experiments

Ca^{2+} indicators were included in the patch-pipettes (at the concentration indicated before) allowing the diffusion into the cells. The preparation was illuminated with a blue LED system (Tolket) through the epifluorescence port of the widefield microscope, and images were acquired using an Andor iXon 885 camera controlled through a Till Photonics interface system. The focal plane was set close to the basal pole of OHCs where synapses are found. The signal-to-noise ratio was improved with an on-chip binning of 4 × 4, giving a resolution of 0.533 µm/pixel with the 60× water immersion objective. The image size

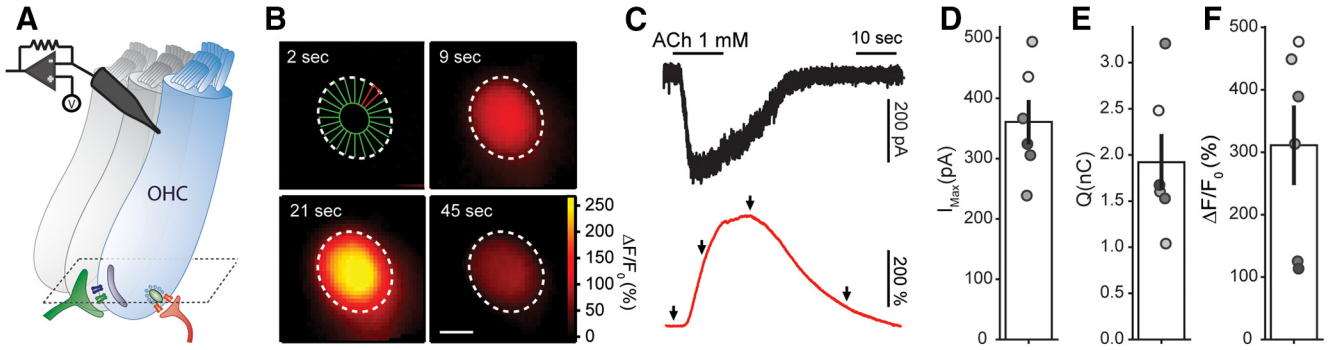

Figure 1. ACh evokes global Ca^{2+} transients in OHCs. ***A***, Illustration of a recorded OHCs within the intact organ of Corti preparation, with synaptic connections (green MOC terminal, red Type II afferent), and a scheme of the imaging focal plane (dashed lines). ***B***, Sequence of wide-field microscopy images of an OHC (loaded with Fluo-4) during ACh 1 mM perfusion. Dotted white lines represent the outer margin of the OHC's fluorescence signal. First image shows ROI design scheme in which the cell's cytoplasm was divided in 24 radial ROIs (see Materials and Methods). Scale bar: 5 μm. ***C***, Black trace corresponds to the whole-cell current recorded during ACh perfusion (Vhold = −100 mV) and red trace to the $\Delta F/F_0$ signal measured at the ROI depicted in red on panel ***B***. Arrows indicate the time points of images shown on panel ***B***. ***D–F***, Peak current (***D***), charge (***E***), and maximal $\Delta F/F_0$ (***F***) during ACh perfusion. Bar plots are mean ± SEM.

was set to 50 × 50 pixels which allowed an acquisition rate of 140 frames/s. Image acquisition started 5 min after whole-cell break in to ensure the proper dialysis of the cell content and lasted up to 45 min. Images were analyzed with custom-written routines in IgorPro 6.37 (Wavemetrics).

A time lapse consisting of 250 images were taken for each experiment. An averaged image in each time lapse was used to determine the edge of the cell by an automatic thresholding algorithm. Within the cell borders, a donut-shaped mask covering the cell's cytoplasm was defined comprising 40–90% of the maximal fluorescence signal. The mask was divided in 24 radial regions of interest (ROIs) with its center set at the maximal intensity pixel of the cell. Fluorescence intensity was measured in every ROI for each time frame as $\Delta F/F_0$, or ΔF in cases where experimental treatments produced an effect on basal fluorescence (F_0). Normalization by F_0 is less critical in our experimental conditions provided that dye concentration is homogeneous throughout the imaging area (OHCs' cytoplasm), and also across recordings (always set by intracellular solution, 400 μM; Bootman et al., 2013). Two criteria were used to determine that a successful synaptic Ca^{2+} event occurred at a particular ROI: (1) a fluorescence peak was identified right after the MOC stimulus, with 2.5× higher amplitude than the standard deviation of the baseline fluorescence; and (2) the area under the curve (fluorescence trace) was larger than 0.11 [arbitrary units (A.U.)/s]. Finally, those ROIs that exhibited a consistent pattern of activation were selected as hotspots and used for further analysis of the fluorescence signal. Photobleaching was corrected for long acquisition protocols by fitting a line between prestimulus baseline and final fluorescence.

To determine the spread of the fluorescence change across the OHC cytoplasm, the response image when the fluorescence signal peaked was normalized to prestimulus fluorescence. Then, it was thresholded by fitting a bimodal distribution to the image histogram and the area and center of mass of the resulting mask calculated. Signal spread area was divided by the cell total area for comparison. The center of mass, which takes into account not only the area of the signal but also the fluorescence intensity in each point, was used to determine the location of the Ca^{2+} entry sites (both MOC and VGCC), and thus the distance between them.

Statistical analysis

Data are presented as group mean ± SEM and were analyzed with Infostat (Universidad Nacional de Córdoba). Effect sizes were calculated using R Statistical Software (RRID:SCR_001905) and the statsExpressions package. The presence of outlier datapoints was evaluated with Grubb's test. The Mann–Whitney test was used to perform comparisons between two groups and Kruskal-Wallis one-way analysis of variance followed by Conover's test for comparisons between multiple groups (non-corrected). Wilcoxon signed-rank and Friedman's test were used for comparisons between two and multiple paired samples, respectively. Non-parametric statistics were preferred given our sample sizes and the impossibility of testing the assumptions of parametric procedures. r value was used to inform effect sizes for comparison between two groups and ϵ^2 value for comparison between multiple groups. Kendall's W was used to inform effect sizes for comparison between multiple paired samples. F test was used to compare models fitting in Figure 5*C*. Differences between samples were considered significant when $p < 0.05$.

Results

Local ACh application evokes a global Ca^{2+} rise in OHCs

To directly measure Ca^{2+} influx and spread by activation of $\alpha9\alpha10$ receptors, the Ca^{2+}-sensitive indicator Fluo-4 was loaded into cells through the patch-clamp electrode (Fig. 1*A*). In a first approach, a local application pipette was used to puff ACh onto the organ of Corti preparation. Figure 1*B* presents a series of images taken at the OHCs base, before and after ACh application (Fig. 1*A* for representation of imaging focal plane). The first image in the sequence also shows an array of ROIs designed to measure fluorescence changes in the cytoplasm as a function of time (% $\Delta F/F_0$, unless otherwise indicated). The application of a nearly saturating ACh concentration (1 mM; Lioudyno et al., 2004; Gómez-Casati et al., 2005) produced a global and long lasting elevation of cytoplasmic Ca^{2+} (images in Fig. 1*B*; and traces of fluorescence intensity as a function of time in Fig. 1*C*). The mean peak of the $\Delta F/F_0$ signal was 311 ± 65%, with a corresponding electrophysiological response integral of 1.9 ± 0.3 nC ($n = 6$; Fig. 1*C–E*). These values were considered as an upper limit of efferent activation, since this very high concentration of an externally applied agonist activates receptors distributed throughout the surface of the cell and bypasses presynaptic synaptic vesicle availability.

Cholinergic synaptic Ca^{2+} signals in OHCs

An alternative and more physiological approach to investigate efferent input to OHCs was undertaken by electrically stimulating MOC axons innervating these cells, to evoke ACh synaptic release. Figure 2*A* shows a series of images of an OHC during a typical protocol of MOC fibers stimulation. In contrast to that observed with ACh external applications, local and brief Ca^{2+} transients were seen in response to synaptic activation. Only one Ca^{2+} entry site was observed in each recorded OHC ($n = 6$ cells). Representative traces of fluorescence changes at the brightest ROI are shown in the bottom panel of Figure 2*B*, red traces, whereas the corresponding synaptic currents recorded in the

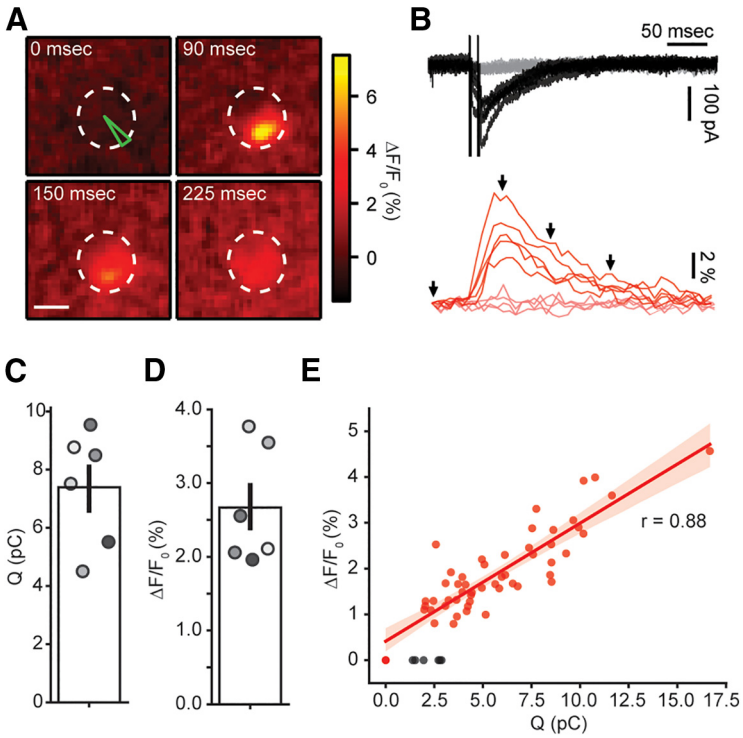

Figure 2. Efferent fiber electrical stimulation evokes localized Ca^{2+} signals in OHCs. ***A***, Sequence of images showing the localized Ca^{2+} increase in an OHC following efferent fiber stimulation. Scale bar: 5 μm. ***B***, top, Representative whole-cell current traces during doble-pulse efferent electrical stimulation at 100 Hz (Vh = −100 mV). Black traces represent those trials where an eIPSC was detected after the stimulus artifact (failures, in gray). Bottom, Representative Ca^{2+} transients taken at the ROI indicated in green on panel ***A***, for the same trials shown on the top panel. Red traces correspond to trials were an IPSC was detected and failures in pink. ***C***, ***D***, Mean charge (***C***) and $\Delta F/F_0$ (***D***) for successful efferent fiber stimulation trials. Bar plots are mean ± SEM. ***E***, Size of Ca^{2+} transients as function of charge during efferent stimulation trials in a representative OHC. Black dots represent successful IPSC events with no detectable fluorescence signal.

same trials are included in the top panel (black traces). $\alpha9\alpha10$ receptors are highly Ca^{2+} permeable, but because of the much higher concentration of Na^+ and K^+ in the extracellular solution (150 mM of Na^+ plus K^+ vs 1.3 mM Ca^{2+}; see Materials and Methods), the majority of the current allowed in physiological conditions is carried by monovalent cations (Weisstaub et al., 2002). Two technical measures contributed to improve the detection of the Ca^{2+} transients: the use of a high affinity indicator (Fluo-4) to resolve small changes in Ca^{2+} concentration; and the transient voltage-clamping at −100 mV (see Materials and Methods) to maximize Ca^{2+} driving force. Thus, under these experimental conditions efferent stimulation produced inward currents as the result of both $\alpha9\alpha10$ receptors and SK2 channels activation (K^+ equilibrium potential: ∼−82 mV). In addition, paired pulses were used instead of single stimuli to increase the otherwise very low synaptic release probability (Ballestero et al., 2011; Vattino et al., 2020). Because of frame rate limitations, the imaging signal appears as the ensemble activation in response to both stimuli in a pair. An average of 100 ± 22 stimulation trials was performed per cell (range 60–200, $n = 6$ cells), with a synaptic success rate of 87 ± 3% (range: 73–98%, $n = 6$), judged by the presence of IPSCs (see Materials and Methods). In turn, Ca^{2+} signals were detected in 83 ± 5% (range: 64–99%, $n = 6$) of trials with successful synaptic currents. The average Ca^{2+} signal obtained with this protocol presented an amplitude of 2.7 ± 0.3% $\Delta F/F_0$ ($n = 6$ cells), whereas the integral of the synaptic currents was 7.4 ± 0.8 pC, excluding synaptic failures for the calculation of both averages ($n = 6$; Fig. 2*C*,*D*). Imaging and electrophysiological results were highly correlated, as shown in Figure 2*E* ($r = 0.88$ in this representative example, range: 0.65–0.95, $n = 6$). This strong correlation indicates that the imaging signal is a good proxy for $\alpha9\alpha10$ and SK2 synaptic activation, most likely reflecting Ca^{2+} influx through nicotinic receptors. Note that failures in detecting imaging events coincided with the smallest IPSCs (Fig. 2*E*, black symbols).

Synaptic Ca^{2+} signals during trains of efferent stimuli

MOC neurons can be activated as a result of a feedback loop starting in the afferent pathway and producing steady firing of efferent neurons at rates of up to 200 s^{-1} (Liberman, 1988; Brown, 1989; Guinan, 2006). Repetitive activation of MOC axons results in presynaptic facilitation of neurotransmitter release (Ballestero et al., 2011). To explore how train stimulation affects synaptic Ca^{2+} transients, MOC fibers were stimulated at 20, 40, and 80 Hz (300-ms duration each; Fig. 3). Images included in Figure 3*A* were taken at the peak of the Ca^{2+} rise for each train, whereas Figure 3*B* shows average synaptic currents (top, in black) and the corresponding Ca^{2+} signals (bottom, in red) taken at the brightest ROI in each cell. Ca^{2+} levels varied with the frequency of the stimulation train, with average amplitudes of 5.1 ± 1.1% $\Delta F/F_0$, 9.5 ± 2.2% $\Delta F/F_0$ and 15.6 ± 2.5% $\Delta F/F_0$ at 20, 40, and 80 Hz, respectively ($n = 8$; $W_{kendall} = 0.706$, $k = 3$; $p = 0.0001$ Friedman's test; Fig. 3*C*). The integral of the ensemble synaptic response across the duration of the train was 23.6 ± 6.2 pC, 43.3 ± 11.0 pC and 64.1 ± 8.8 pC ($n = 8$; $W_{kendall} = 0.937$, $k = 3$; $p < 0.0001$ Friedman's test; Fig. 3*D*). A positive correlation was observed between the integral of synaptic currents elicited by trains at different frequencies and the amplitude of Ca^{2+} transients ($r = 0.88$; Fig. 3*E*). Moreover, whereas trains at 20 Hz elicited a localized Ca^{2+} rise with a measurable spread within the OHCs cytoplasm of 31 ± 5% (25.9 ± 4.8 μm^2) of the total imaged area (74.0 ± 8.8 μm^2), this value increased to 48 ± 6% (32.1 ± 4.4 μm^2) and 63 ± 5% (43.8 ± 4.0 μm^2) for 40 and 80 Hz, respectively ($n = 8$; $W_{kendall} = 0.762$, $k = 3$; $p < 0.0001$ Friedman's test; Fig. 3*F*).

Comparing Ca^{2+} signals in Figures 1–3, it becomes clear that synaptic activation of $\alpha9\alpha10$ receptors during trains is (at least) ∼20 times smaller than that obtained with locally applied ACh. This might result from the low release probability of MOC terminals (Ballestero et al., 2011; Vattino et al., 2020), in addition to the fact that the stimulation paradigm typically activates a single axon (see Materials and Methods). Moreover, activation by external ACh does not rely on vesicle availability and likely activates both synaptic and extrasynaptic receptors in OHCs. This drastic difference in measurable $\Delta F/F_0$ amplitude between exogenous ACh application (Fig. 1) and electrical stimulation (Figs. 2, 3) suggests that the Ca^{2+} indicator used in these experiments does not saturate even with high-frequency synaptic trains. The tight correlation between ΔF/F and charge in Figure 3*E* further supports this conclusion.

In order to obtain a better understanding of Ca^{2+} dynamics during sustained MOC activity, trains of stimuli at 80 Hz were applied for longer periods of time (0.3–3 s; Fig. 3*G*,*H*).

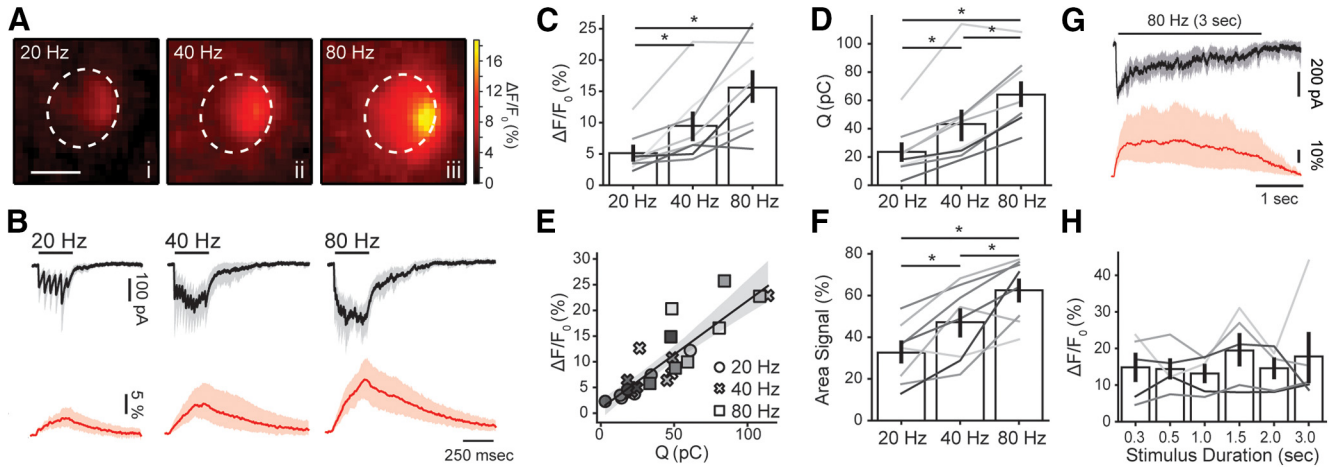

Figure 3. Amplitude and spread of efferent Ca^{2+} transients are dependent on stimulation frequency. ***A***, Representative images of an OHC at the peak of the fluorescence signal during efferent fiber electrical stimulation at 20 (***i***), 40 (***ii***), and 80 (***iii***) Hz. ***B***, Mean inhibitory current traces (black, 95% confidence intervals in gray) recorded during 300 ms efferent fiber electrical stimulation at 20, 40, and 80 Hz (Vh = −100 mV). Red traces show the mean $\Delta F/F_0$ (95% confidence intervals in light red) at the ROI with the highest fluorescence signal. Peak Ca^{2+} values (***C***) and charge (***D***) for 300-ms stimulation trains at tested frequencies. ***E***, Amplitude of fluorescence signal as a function of charge. Each symbol represents a different stimulation frequency. ***F***, Spread of the Ca^{2+} signal within each OHC cytoplasmic space (as percentage of the area in the imaged plane). Values were taken at the time point where the signal peaked. ***G***, Mean whole-cell synaptic response (black, 95% confidence intervals in gray) and Ca^{2+} signals (red, 95% confidence intervals in light red) obtained during a 3-s electrical stimulation of efferent fibers at 80 Hz. ***H***, Peak fluorescence amplitude for trains with duration between 0.3 and 3 s (at 80 Hz). Bar plots are mean ± SEM. Friedman's test; $*p < 0.05$.

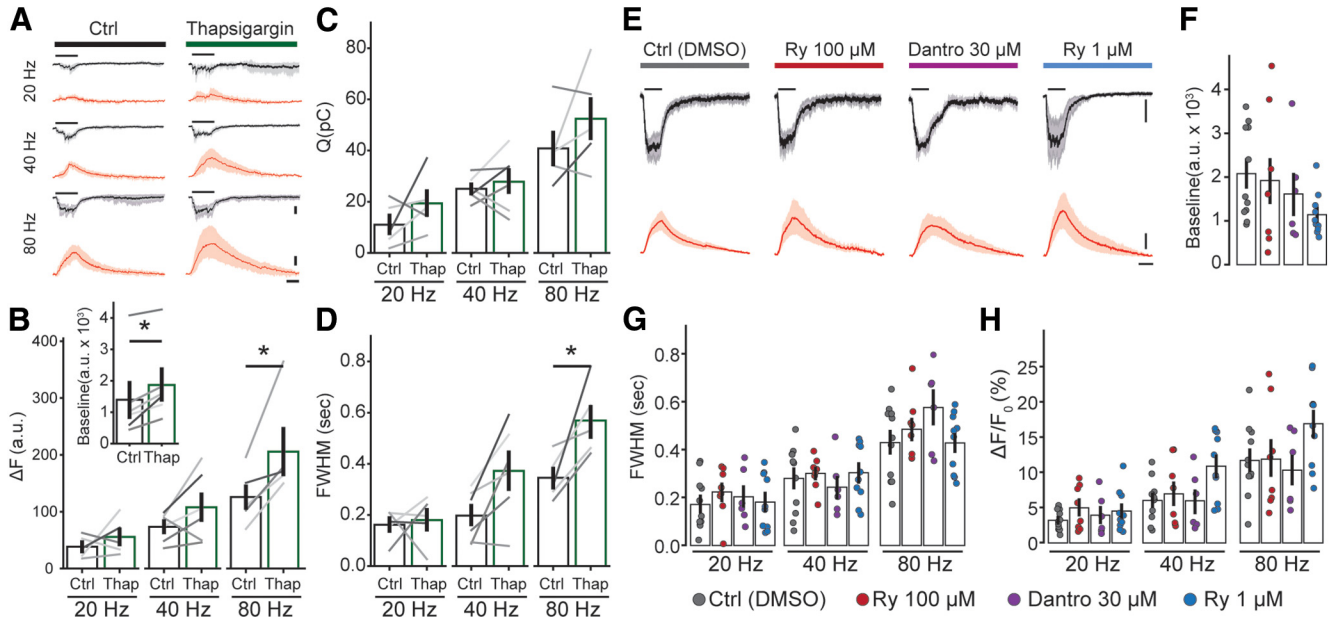

Figure 4. Efferent Ca^{2+} signals are affected by blocking cisternal ATPases, but not by modulators of RyRs. ***A***, Mean synaptic responses (black, 95% confidence intervals in gray) and Ca^{2+} transients (red, 95% confidence intervals in light red) during a 300-ms electrical stimulation at 20, 40, and 80 Hz before and after perfusion of thapsigargin (*x* scale bar: 250 ms; *y* scale bar: 50 A.U. and 100 pA). ***B***, Peak of Ca^{2+} transients (as ΔF). ***C***, Charge of synaptic responses. ***D***, Duration of Ca^{2+} transients (as FWHM). Inset, Baseline fluorescence signal before and after perfusion of thapsigargin. ***E***, Synaptic currents (mean, black, confidence intervals in gray) and Ca^{2+} transients (red, confidence interval in light red) obtained during efferent fiber stimulation (300 ms, 80 Hz), using an intracellular solution containing vehicle (DMSO), RyR blockers (ryanodine 100 μM or dantrolene 30 μM), or a RyR agonist (ryanodine 1 μM; *x* scale bar: 250 ms; *y* scale bar: 50% and 100 pA). ***F***, Baseline fluorescence for each condition. Duration (FWHM; ***G***) and maximal fluorescence signal (as $\Delta F/F_0$; ***H***) for each intracellular solution. Bar plots are mean ± SEM. Wilcoxon signed-rank test; $*p < 0.05$.

A sustained Ca^{2+} load was observed in each of these train durations, but peak values did not differ ($n = 5$; $W_{kendall} = 0.5$, $k = 6$; $p = 0.57$ Friedman's test; Fig. 3*H*). This latter result suggests that OHCs have a tight mechanism for controlling Ca^{2+} overload and spread at high-frequency efferent stimulation. The role of the subsynaptic cistern in this phenomenon has been suggested in the past (Sridhar et al., 1997; Evans et al., 2000; Lioudyno et al., 2004) and was evaluated in the following section.

Modulation of efferent Ca^{2+} transients by subsynaptic cisterns

SERCA pumps, located in OHCs subsynaptic cisterns, have been suggested to modulate synaptic currents through $\alpha9\alpha10$ receptors (Lioudyno et al., 2004). To address a possible role of SERCA in shaping Ca^{2+} transients, the specific blocker thapsigargin (1 μM) was added to the bath during an OHC recording. In the absence of any stimulation, the basal fluorescence increased when perfusing thapsigargin from a control value of 1396 ± 551

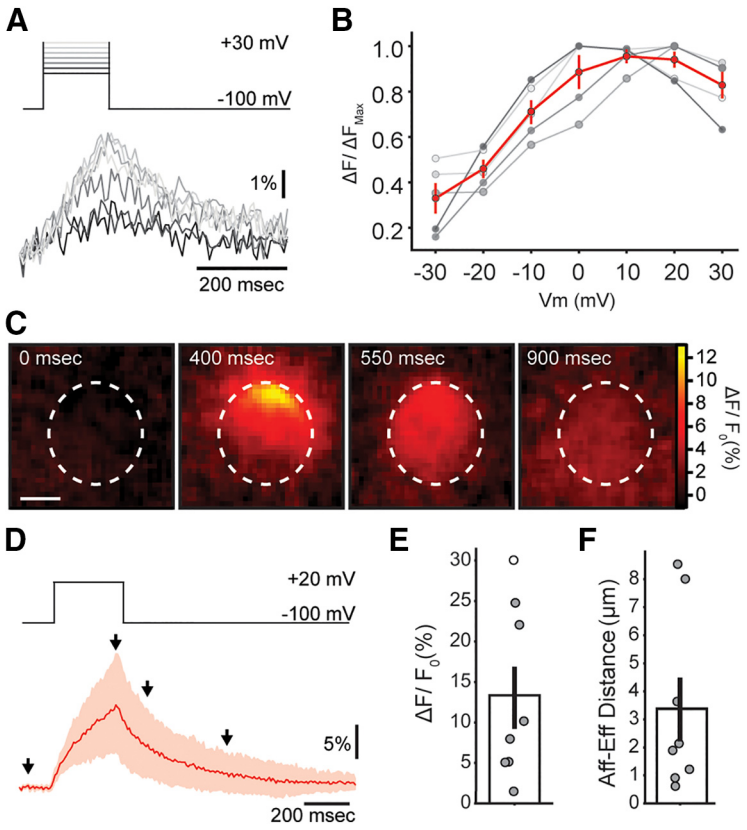

Figure 5. Ca^{2+} transients during VGCC activation in OHCs. ***A***, Representative traces of Ca^{2+} transients measured at the brightest ROI, for voltage steps between −30 and + 30 mV. ***B***, Normalized maximum for Ca^{2+} transients in each cell (gray symbols) as a function of voltage. Red trace and marks represent mean ± SEM. ***C***, Sequence of images showing the localized Ca^{2+} concentration increase in an OHC during 300-ms depolarization to +20 mV. Scale bar: 5 μm. ***D***, Mean trace of the Ca^{2+} signal (in red, 95% confidence interval in light red) during a step pulse to +20 mV (top panel). ***E***, Average $\Delta F/F_0$ for +20-mV steps in OHCs. ***F***, Average distance between locations of afferent (VGCC) and efferent (MOC) Ca^{2+} signals within each OHC. Bar plots are mean ± SEM. Friedman's test; *$p < 0.05$.

to 1851 ± 502 A.U. ($n = 6$; $r = 0.898$; $p = 0.024$ Wilcoxon test; Fig. 4*B*, inset). This ~30% increase in the basal cytoplasmic concentration of Ca^{2+} might represent the basal SERCA activity responsible for pumping ions out of the OHC cytoplasm at rest.

In a following set of experiments, trains of MOC stimuli were applied before and during the application of thapsigargin (Fig. 4*A–D*). Peak ΔF values were calculated instead of $\Delta F/F_0$ (Fig. 4*B*), to avoid an incorrect estimation of Ca^{2+} transients size that would result from dividing ΔF by a larger basal fluorescence in the presence of thapsigargin. A similar approach using ΔF has been applied in the past to avoid misleading calculations of Ca^{2+} transients size (Kennedy, 2002; Frank et al., 2009; Moglie et al., 2018; see Materials and Methods). Synaptic currents integral are shown in Figure 4*C*. As previously described for $\Delta F/F_0$ (Fig. 3), peak ΔF values increased with the frequency of stimulation in control conditions: 38.4 ± 8.6, 73.4 ± 10.5, and 125.9 ± 21.8 A.U. for 20-, 40-, and 80-Hz trains ($n = 5$, $p = 0.0085$ Friedman's test). In the presence of thapsigargin, ΔF values grew to 55.8 ± 14.1, 107.9 ± 24.5, and 205.7 ± 39.9 A.U. for 20, 40, and 80 Hz, respectively ($n = 6$), showing statistically significant differences for the 80-Hz train compared with control ($r_{20\ Hz} = 0.301$, $r_{40\ Hz} = 0.641$, $r_{80\ Hz} = 0.903$; $p = 0.04$, Wilcoxon signed-rank test).

The effect of thapsigargin on the duration of the synaptic Ca^{2+} transients was analyzed, by measuring the full width at half maximum (FWHM) of the signal. In control conditions, FWHM values varied with the stimulation frequency: 162 ± 27 ms at 20 Hz, 198 ± 42 ms at 40 Hz, and 345 ± 38 ms at 80 Hz ($n = 5$; $p = 0.0097$, Friedman's test). For the 20 Hz trains, the FWHM of the transient was largely shorter than the stimulating train duration (300 ms) because of sporadic synaptic activation. Thapsigargin prolonged Ca^{2+} transients with average values of 180 ± 42 ms at 20 Hz, 372 ± 75 ms at 40 Hz and 569 ± 62 ms at 80 Hz ($n = 5$; $r_{20\ Hz} = 0.06$, $r_{40\ Hz} = 0.812$, $r_{80\ Hz} = 0.903$; $p = 0.048$ Wilcoxon signed-ranked test for the 80-Hz train compared with control). Taken together, these results indicate that SERCA pumps, most likely present at subsynaptic cistern (Lioudyno et al., 2004), play a significant role in accelerating the removal of Ca^{2+} entering through $\alpha9\alpha10$ at efferent synapses and also in curtailing the peak of the transient.

Since the presence of RyR has been described morphologically, and indirectly through the modulation of MOC-OHC synaptic function by ryanodine (Evans et al., 2000; Lioudyno et al., 2004; Grant et al., 2006), in the following experiments we directly tested Ca^{2+} dynamics at efferent synapses in the presence of drugs that modulate RyR. To avoid indirect or presynaptic effects (Zhang et al., 2020), drugs were included in the patch pipette (control experiments were performed in the presence of vehicle, DMSO). Low (1 μM) and high (100 μM) concentrations of ryanodine were used to either activate or block RyR (McGrew et al., 1989; Lanner et al., 2010). Dantrolene, a specific inhibitor of these receptors, was also tested. Interestingly, none of these treatments showed any effect on either the amplitude of synaptic Ca^{2+} transients ($\epsilon^2_{20\ Hz} = 0.04/p_{20\ Hz} = 0.70$, $\epsilon^2_{40\ Hz} = 0.19/p_{40\ Hz} = 0.08$, $\epsilon^2_{80\ Hz} = 0.17/p_{80\ Hz} = 0.25$; Kruskal–Wallis test; same for ΔF; Fig. 4*E*, *H*), duration (estimated as FWHM; $\epsilon^2_{20\ Hz} = 0.04/p_{20\ Hz} = 0.72$, $\epsilon^2_{40\ Hz} = 0.04/p_{40\ Hz} = 0.71$, $\epsilon^2_{80\ Hz} = 0.12/p_{80\ Hz} = 0.13$; Kruskal–Wallis test; Fig. 4*E*,*G*), or basal Ca^{2+} ($\epsilon^2 = 0.12$; $p = 0.24$ Kruskal–Wallis test; Fig. 4*F*). The corresponding values for these experiments are shown in Table 1. These results preclude the participation of RyR in the modulation of OHCs efferent responses.

Ca^{2+} entry through L-type Ca^{2+} channels

Ca^{2+} influx through VGCC was investigated by applying step depolarizations to OHCs, from a holding potential of −100 mV, up to a range of potentials between −30 and +30 mV. Representative Ca^{2+} transients are shown in Figure 5*A*, with peak values that followed the expected bell-shaped dependence on membrane potential, and maxima at +10/+20 mV (Fig. 5*B*). Only one Ca^{2+} entry spot was observed per OHC in these experiments.

Step depolarizations to +20 mV for 300 ms (same duration as that of MOC train stimulation in Figs. 3, 4) evoked Ca^{2+} transients with an average peak of 13.3 ± 3.8% $\Delta F/F_0$, with highly variable values that ranged from 1.5% to 30.1% $\Delta F/F_0$. This average matched in size with transients obtained with 40 and 80 Hz

Table 1. Values for integral of synaptic currents, amplitude and duration Ca^{2+} signals during step depolarization of OHCs or MOC stimulation at 20-, 40-, and 80-Hz trains, in different pharmacological conditions

		Q (pC)	$\Delta F/F_0$ (%)	FWHM (s)
Depolarization	Ctrl (DMSO)	—	3.3 ± 0.8 (n = 10)	0.22 ± 0.04 (n = 7)
	Ryanodine 100 μM	—	6.4 ± 1.9 (n = 7)	0.21 ± 0.08 (n = 7)
	Dantrolene 30 μM	—	13.2 ± 4.7 (n = 7)	0.27 ± 0.07 (n = 7)
	Ryanodine 1 μM	—	15.8 ± 3.5 (n = 10)	0.35 ± 0.02 (n = 10)
20 Hz	Ctrl (DMSO)	20.0 ± 4.0 (n = 11)	3.2 ± 0.4 (n = 11)	0.17 ± 0.03 (n = 11)
	Ryanodine 100 μM	20.6 ± 3.5 (n = 8)	5.0 ± 1.1 (n = 8)	0.22 ± 0.04 (n = 8)
	Dantrolene 30 μM	12.8 ± 2.0 (n = 6)	3.9 ± 1.2 (n = 6)	0.20 ± 0.04 (n = 6)
	Ryanodine 1 μM	17.1 ± 4.9 (n = 10)	4.5 ± 0.9 (n = 10)	0.18 ± 0.04 (n = 10)
40 Hz	Ctrl (DMSO)	34.3 ± 5.0 (n = 11)	6.0 ± 1.8 (n = 11)	0.28 ± 0.04 (n = 11)
	Ryanodine 100 μM	31.6 ± 4.4 (n = 8)	7.0 ± 1.6 (n = 8)	0.30 ± 0.02 (n = 8)
	Dantrolene 30 μM	25.6 ± 3.3 (n = 6)	6.0 ± 1.7 (n = 6)	0.24 ± 0.05 (n = 6)
	Ryanodine 1 μM	37.1 ± 6.3 (n = 10)	10.9 ± 1.5 (n = 10)	0.30 ± 0.04 (n = 10)
80 Hz	Ctrl (DMSO)	61.2 ± 6.3 (n = 11)	11.7 ± 1.6 (n = 11)	0.43 ± 0.05 (n = 11)
	Ryanodine 100 μM	47.7 ± 5.7 (n = 8)	11.9 ± 2.6 (n = 8)	0.49 ± 0.04 (n = 8)
	Dantrolene 30 μM	42.4 ± 2.1 (n = 6)	10.3 ± 2.2 (n = 6)	0.58 ± 0.07 (n = 6)
	Ryanodine 1 μM	60.3 ± 6.7 (n = 10)	16.9 ± 1.9 (n = 10)	0.43 ± 0.04 (n = 10)

MOC trains (n = 8; $p_{20\ HZ}$ = 0.02, $p_{40\ Hz}$ = 0.82, p_{80Hz} = 0.37, Friedman's test; $W_{Kendall}$ = 0.263, k = 4; Figs. 3*C*, 5*C–E*). Moreover, the spread of the fluorescence signal was also equivalent to that observed with the 40- and 80-Hz trains of efferent stimulation [57 ± 7% of OHC area (36.0 ± 3.2 μm^2); $p_{20\ HZ} < 0.001$, $p_{40\ Hz}$ = 0.37, p_{80Hz} = 0.37, Friedman's test; $W_{Kendall}$ = 0.692, k = 4].

Previous evidence indicates that Type II afferents on OHCs are closely positioned with efferent synapses and subsynaptic cisterns (Fuchs et al., 2014; Saito, 1980, 1990). A functional quantification of this proximity was evaluated by measuring the physical distance between the centers of mass of VGCC and MOC Ca^{2+} transients within a given cell (see Materials and Methods; Fig. 5*C*,*F*). An average value of 3.7 ± 1.1 μm (n = 8) was estimated, ranging from 0.6 to 8.5 μm, with five out of eight cells showing values ≤2 μm. Because of the proximity of VGCC Ca^{2+} signals to synaptic cisterns, and the large spread, the possible modulation by SERCA and RyR was further investigated.

No changes in the amplitude of the depolarization-evoked Ca^{2+} signals were observed in the presence of the SERCA blocker thapsigargin (control ΔF: 68 ± 24 A.U., thapsigargin ΔF: 53 ± 9, n = 5; r = 0.30; p = 0.58 Wilcoxon signed-rank test; Fig. 6*A*,*B*). In addition, neither 100 μM ryanodine nor dantrolene modified VGCC signals (6.4 ± 1.9% $\Delta F/F_0$; n = 7; p = 0.344 Kruskal–Wallis test, and 13.2 ± 4.7% $\Delta F/F_0$; n = 7; p = 0.073 Kruskal–Wallis test, respectively) indicating that CICR was not elicited during +20 mV voltage pulses in our recording conditions. In contrast, 1 μM ryanodine, a concentration known to increase RyR opening time (McGrew et al., 1989), elicited a strong potentiation of the Ca^{2+} transient, with average peak values of 15.8 ± 3.5% $\Delta F/F_0$, compared with 3.3 ± 0.8% $\Delta F/F_0$ in control experiments with vehicle (DMSO) in the pipette (n = 10 and n = 7, respectively; p = 0.001 Kruskal–Wallis test, and also p = 0.046 compared with 100 μM ryanodine; ϵ^2 = 0.34; Fig. 6*C*, *D*), suggesting that RyR can be recruited during VGCC Ca^{2+} events. Taken together, these data suggest that VGCC Ca^{2+} transients are not controlled by SERCA pumps, but could be modulated by RyR present in synaptic and/or lateral wall cisterns (Lioudyno et al., 2004; Grant et al., 2006).

Discussion

The present results provide a direct analysis of synaptic Ca^{2+} dynamics in OHCs triggered by MOC (efferent) and VGCC (afferent) activation. It also shows evidence for cisternal modulation of amplitude, spread, and duration of Ca^{2+} transients. Significantly, only one efferent Ca^{2+} hotspot was found per OHC, suggesting that a single MOC fiber is stimulated at a time, although more MOC-OHC synaptic contacts are present (Liberman, 1990; Warr, 1992). The amplitude of Ca^{2+} transients shows a strong dependence on MOC stimulation at frequencies between 20 and 80 Hz (Fig. 3), which might explain the reported changes in MOC inhibitory strength as a function of stimulation rate (Galambos, 1956; Art et al., 1984; Gifford and Guinan, 1987). On the other hand, a single Ca^{2+} spot was also observed when activating VGCC by step depolarizations, although multiple contacts with Type II afferent coexist in one OHC within a close proximity (Fuchs and Glowatzki, 2015). Moreover, although Ca^{2+} signals produced by activation of VGCC were similar in amplitude to those through $\alpha9\alpha10$ receptors, they were significantly smaller to those reported for IHCs (Frank et al., 2009; Wong et al., 2013; Moglie et al., 2018). This most likely relates to the weak capacity of OHCs to release neurotransmitter and activate Type II afferents compared with the multivesicular release from IHC ribbon synapse, responsible for encoding timing, intensity and frequency in each Type I afferent fiber (Fuchs and Glowatzki, 2015).

Ca^{2+} homeostasis in OHCs and efferent regulation

Several studies have reported alternative mechanisms that operate in OHCs to handle Ca^{2+} influx, with special attention on Ca^{2+} entering through MET channels (Fettiplace and Nam, 2019). Thus, the integrity of OHCs and cochlear function relies on the normal operation of mechanisms such as buffering and extrusion by plasma membrane ATPases present in stereocilia (Kozel et al., 1998; Tong et al., 2016). In addition, mitochondria, abundantly found in a layer right below the cuticular plate in OHCs, play the important role of containing Ca^{2+} leak into the basolateral compartment (Furness and Hackney, 2006; Beurg et al., 2010).

In MOC synapses located at the basal pole of OHCs, Ca^{2+} influx through $\alpha9\alpha10$ receptors rapidly activates SK2 channels at the plasma membrane because of a tight functional coupling (Oliver et al., 2000). The large synaptic cisterns located at a close physical distance of OHCs plasma membrane determines a restricted diffusion space where Ca^{2+} ions entering through $\alpha9\alpha10$ accumulate (Fuchs et al., 2014). However, since efferent fibers operate best at prolonged and high-frequency MOC

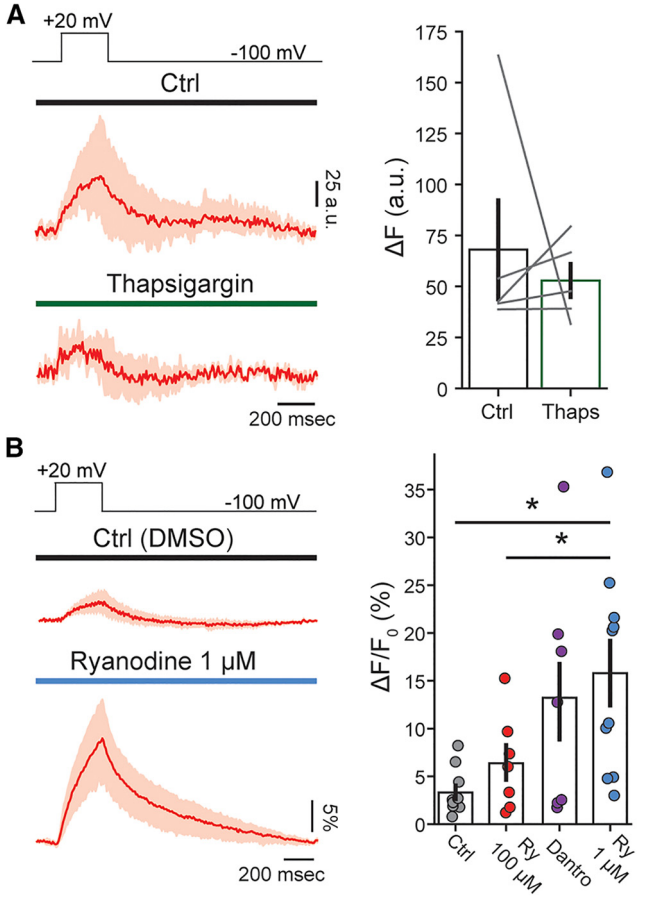

Figure 6. Modulation of afferent Ca^{2+} influx through VGCC by thapsigargin and ryanodine. ***A***, Mean traces of the Ca^{2+} transients obtained with 300-ms depolarization to +20 mV before (top) and during perfusion of thapsigargin (bottom). On the right, average peak Ca^{2+} level (ΔF) for step depolarizations. ***B***, Mean traces of the Ca^{2+} transients during with steps to +20 mV, using intracellular solutions containing DMSO or ryanodine 1 μM. Average peak Ca^{2+} signal ($\Delta F/F_0$) are shown on the right for experimental conditions in low and high concentrations of ryanodine (Ry; 1 and 100 μM) and dantrolene (30 μM). Wilcoxon signed-rank test; *$p < 0.05$.

activation (Robertson and Gummer, 1985; Brown, 1989), the physical barrier provided by the synaptic cisterns might not be sufficient to prevent Ca^{2+} leak onto OHCs cytoplasm. The confinement of efferent Ca^{2+} might be crucial to avoid interaction with off targets, such as activation of exocytosis at Type II afferent synapses (see below), modulation of prestin-driven electromotility (Dallos et al., 1997; Frolenkov et al., 2000), or even excitotoxicity (Choi, 1995). The present results provide evidence indicating that at high-frequency efferent stimulation cisternal ATPases (SERCA) come into play to control excessive Ca^{2+} spread and prevent its spill over. This effect of cisternal ATPases is strongest at 80-Hz trains, a condition that leads to the largest Ca^{2+} load.

It should be noted that, because of the small domain determined by OHCs plasma membrane and synaptic cisterns, and also the spread of the Ca^{2+} transients (Fig. 3*F*), it is very likely that under our experimental conditions Ca^{2+} signals recorded at high-frequency MOC stimulation result, at least partially, from Ca^{2+} that escaped into the cytoplasm. Nevertheless, one should take into account that under normal physiological conditions the high concentration of intracellular buffers (Sakaguchi et al., 1998; Hackney et al., 2005) might restrain Ca^{2+} diffusion. Moreover, because of the fragility of the tissue, as well as the instability of OHCs recordings from older animals, experiments were performed within the postnatal day (P)12–P14 age range and room temperature. Therefore, some of our conclusions may differ in more mature OHCs and/or at body temperature.

Our results do not provide support for the participation of RyR during MOC activation within a wide range of stimulation strengths (20- to 80-Hz trains of 300 ms of duration). This result contrasts with previous observations in OHCs in which the role of RyR was evaluated indirectly by measuring efferent synaptic activation (Lioudyno et al., 2004). We cannot preclude that RyR might engage if preceded by hair cell excitation, which firstly raises cytoplasmic Ca^{2+} concentration, and as a consequence of this paves the way for cisternal load through SERCA activity. This mechanism has been proposed to occur in chick and immature hair cells from rats (Im et al., 2014; Zachary et al., 2018), but whether it is relevant in OHCs remains to be proven. The observation that MOC inhibition *in vivo* is potentiated by a preceding auditory stimulation might indicate that this phenomenon could be functional in hearing (Kujawa and Liberman, 1999).

Ca^{2+} influx through VGCC and Type II afferent activation

Ca^{2+} currents through VGCC in OHCs are several fold smaller than in IHCs and present a shift to the right in the current–voltage relation (Knirsch et al., 2007; Johnson and Marcotti, 2008; Wong et al., 2013). Accordingly, in the present work we show that Ca^{2+} signals peaked at +20 mV (−20 mV for IHCs), and their amplitudes (13.3% $\Delta F/F_0$, 300-ms step) were 3-fold smaller compared with brief depolarizations to submaximal potentials in IHCs (42% $\Delta F/F_0$, 20 ms to −30 mV; Moglie et al., 2018). This result adds to other features of afferent synapses in OHCs indicating that the release probability is small in these cells when compared with IHCs. Thus, ribbons in active zone areas with Type II afferents are small, irregular in shape, and can accommodate few vesicles (Fuchs and Glowatzki, 2015). However, Ca^{2+} transients activated by VGCC were further potentiated by a RyR agonist (Fig. 6), suggesting that CICR mechanisms can boost synaptic strength in contacts with Type II afferents. CICR has been shown to modulate vesicle release and recruitment on afferent synapses of hair cells from frogs and turtles (Lelli et al., 2003; Castellano-Muñoz et al., 2016). The fact that the specific RyR antagonists, dantrolene and ryanodine at high concentrations, failed to inhibit Ca^{2+} transients produced by VGCC activation (Fig. 6*B*) most likely indicates that in our stimulating conditions (300-ms step depolarization to +20 mV) intracellular Ca^{2+} does not reach the critical concentration necessary to trigger CICR processes. Taken together, it can be concluded that VGCC Ca^{2+} transients are susceptible to RyR modulation, but that stronger OHCs excitation is required to evoke CICR in the absence of pharmacological modulators.

Whether RyRs involved in VGCC-mediated Ca^{2+} boost are located in OHCs synaptic cisterns (Lioudyno et al., 2004; Grant et al., 2006), or lateral wall cisterns (Grant et al., 2006; Ranum et al., 2019), or even at other intracellular organelles is still unknown. If RyRs located in sublateral walls cisterns were responsible for VGCC potentiation (Grant et al., 2006; Ranum et al., 2019), an independent functioning of afferent and efferent synapses would be expected. Alternatively, if synaptic cisterns were involved in RyR potentiation of VGCC signals, a close interaction between afferent and efferent synapses could occur in OHCs. Thus, Ca^{2+} entering through $\alpha9\alpha10$ receptors would be taken up by SERCA pumps, filling the cisterns with Ca^{2+} and

providing fuel for boosting transmitter release at Type II afferents through activation of RyRs.

Both functional (Fig. 6*E*) and structural (Saito, 1990; Fuchs et al., 2014) evidence indicates that the diffusion interval between afferent and efferent synaptic locations is very short. This observation together with the finding of a wide cytoplasmic Ca^{2+} spread obtained with high-frequency MOC stimulation (Fig. 3*F*) suggests that efferent to Type II afferent crosstalk in OHCs might occur during efferent activation. In contrast to what was observed in developing IHCs where afferent and efferent Ca^{2+} signals have opposing roles (Moglie et al., 2018), activation of MOC and Type II afferents synapses might both occur in loud environments (Robertson and Gummer, 1985; Brown, 1989; Fuchs and Glowatzki, 2015; Weisz et al., 2021). Therefore, coincident activation of the two synapses onto OHCs, whether causal or not, would not be rare.

In conclusion, in the present work, we show for the first time Ca^{2+} dynamics at the base of OHCs. Interestingly, intracellular cisterns and organelles play important and differential roles in Ca^{2+} transients elicited by the activation of afferent and efferent synaptic signaling.

References

Art JJ, Fettiplace R, Fuchs PA (1984) Synaptic hyperpolarization and inhibition of turtle cochlear hair cells. J Physiol 356:525–550.

Augustine GJ, Santamaria F, Tanaka K (2003) Local calcium signaling in neurons. Neuron 40:331–346.

Ballestero J, Zorrilla de San Martín J, Goutman JD, Elgoyhen AB, Fuchs PA, Katz E (2011) Short-term synaptic plasticity regulates the level of olivocochlear inhibition to auditory hair cells. J Neurosci 31:14763–14774.

Beurg M, Safieddine S, Roux I, Bouleau Y, Petit C, Dulon D (2008) Calcium- and otoferlin-dependent exocytosis by immature outer hair cells. J Neurosci 28:1798–1803.

Beurg M, Fettiplace R, Nam J, Ricci AJ (2009) Localization of inner hair cell mechanotransducer channels using high-speed calcium imaging. Nat Neurosci 12:553–558.

Beurg M, Nam JH, Chen Q, Fettiplace R (2010) Calcium balance and mechanotransduction in rat cochlear hair cells. J Neurophysiol 104:18–34.

Bootman MD, Lipp P, Berridge MJ (2001) The organisation and functions of local Ca2+ signals. J Cell Sci 114:2213–2222.

Bootman MD, Rietdorf K, Collins T, Walker S, Sanderson M (2013) Ca2+-sensitive fluorescent dyes and intracellular Ca2+ imaging. Cold Spring Harb Protoc 8:83–99.

Brown MC (1989) Morphology and response properties of single olivocochlear fibers in the guinea pig. Hear Res 40:93–109.

Castellano-Muñoz M, Schnee ME, Ricci AJ (2016) Calcium-induced calcium release supports recruitment of synaptic vesicles in auditory hair cells. J Neurophysiol 115:226–239.

Chen Q, Mahendrasingam S, Tickle JA, Hackney CM, Furness DN, Fettiplace R (2012) The development, distribution and density of the plasma membrane calcium ATPase 2 calcium pump in rat cochlear hair cells. Eur J Neurosci 36:2302–2310.

Choi DW (1995) Calcium: still center-stage in hypoxic-ischemic neuronal death. Trends Neurosci 18:58–60.

Dallos P (2008) Cochlear amplification, outer hair cells and prestin. Curr Opin Neurobiol 18:370–376.

Dallos P, He DZ, Lin X, Sziklai I, Mehta S, Evans BN (1997) Acetylcholine, outer hair cell electromotility, and the cochlear amplifier. J Neurosci 17:2212–2226.

Dumont RA, Lins U, Filoteo AG, Penniston JT, Kachar B, Gillespie PG (2001) Plasma membrane Ca2+-ATPase isoform 2a is the PMCA of hair bundles. J Neurosci 21:5066–5078.

Elgoyhen AB, Johnson DS, Boulter J, Vetter DE, Heinemann SF (1994) α9: an acetylcholine receptor with novel pharmacological properties expressed in rat cochlear hair cells. Cell 79:705–715.

Elgoyhen AB, Vetter DE, Katz E, Rothlin CV, Heinemann SF, Boulter J (2001) alpha10: a determinant of nicotinic cholinergic receptor function in mammalian vestibular and cochlear mechanosensory hair cells. Proc Natl Acad Sci USA 98:3501–3506.

Engström H (1958) On the double innervation of the sensory epithelia of the inner ear. Acta Otolaryngol 49:109–118.

Evans MG, Lagostena L, Darbon P, Mammano F (2000) Cholinergic control of membrane conductance and intracellular free Ca2+ in outer hair cells of the guinea pig cochlea. Cell Calcium 28:195–203.

Fettiplace R (2017) Hair cell transduction, tuning, and synaptic transmission in the mammalian cochlea. Compr Physiol 7:1197–1227.

Fettiplace R, Nam JH (2019) Tonotopy in calcium homeostasis and vulnerability of cochlear hair cells. Hear Res 376:11–21.

Ficarella R, Di Leva F, Bortolozzi M, Ortolano S, Donaudy F, Petrillo M, Melchionda S, Lelli A, Domi T, Fedrizzi L, Lim D, Shull GE, Gasparini P, Brini M, Mammano F, Carafoli E (2007) A functional study of plasma-membrane calcium-pump isoform 2 mutants causing digenic deafness. Proc Natl Acad Sci USA 104:1516–1521.

Flores EN, Duggan A, Madathany T, Hogan AK, Márquez FG, Kumar G, Seal RP, Edwards RH, Liberman MC, García-Añoveros J (2015) A non-canonical pathway from cochlea to brain signals tissue-damaging noise. Curr Biol 25:606–612.

Frank T, Khimich D, Neef A, Moser T (2009) Mechanisms contributing to synaptic Ca2+ signals and their heterogeneity in hair cells. Proc Natl Acad Sci USA 106:4483–4488.

Frolenkov GI, Mammano F, Belyantseva IA, Coling D, Kachar B (2000) Two distinct Ca(2+)-dependent signaling pathways regulate the motor output of cochlear outer hair cells. J Neurosci 20:5940–5948.

Fuchs PA (1996) Synaptic transmission at vertebrate hair cells. Curr Opin Neurobiol 6:514–519.

Fuchs PA, Glowatzki E (2015) Synaptic studies inform the functional diversity of cochlear afferents. Hear Res 330:18–25.

Fuchs PA, Lehar M, Hiel H (2014) Ultrastructure of cisternal synapses on outer hair cells of the mouse cochlea. J Comp Neurol 522:717–729.

Furness DN, Hackney CM (2006) The structure and composition of the stereociliary bundle of vertebrate hair cells. In: Springer handbook of auditory research. Vertebrate hair cells. New York: Springer US.

Galambos R (1956) Suppression of auditory nerve activity by stimulation of efferent fibers to cochlea. J Neurophysiol 19:424–437.

Gifford ML, Guinan JJ (1987) Effects of electrical stimulation of medial olivocochlear neurons on ipsilateral and contralateral cochlear responses. Hear Res 29:179–194.

Glowatzki E, Fuchs PA (2002) Transmitter release at the hair cell ribbon synapse. Nat Neurosci 5:147–154.

Gómez-Casati ME, Fuchs PA, Elgoyhen AB, Katz E (2005) Biophysical and pharmacological characterization of nicotinic cholinergic receptors in rat cochlear inner hair cells. J Physiol 566:103–118.

Goutman JD, Fuchs PA, Glowatzki E (2005) Facilitating efferent inhibition of inner hair cells in the cochlea of the neonatal rat. J Physiol 566:49–59.

Grant L, Slapnick S, Kennedy HJ, Hackney CM (2006) Ryanodine receptor localisation in the mammalian cochlea: an ultrastructural study. Hear Res 219:101–109.

Guinan JJ (1996) Physiology of olivocochlear efferents. In: The cochlea. (Dallos P, Popper AN, Fay RR, eds). New York: Springer New York, Inc.

Guinan JJ (2006) Olivocochlear efferents: anatomy, physiology, function, and the measurement of efferent effects in humans. Ear Hear 27:589–607.

Hackney CM, Mahendrasingam S, Penn A, Fettiplace R (2005) The concentrations of calcium buffering proteins in mammalian cochlear hair cells. J Neurosci 25:7867–7875.

Im GJ, Moskowitz HS, Lehar M, Hiel H, Fuchs PA (2014) Synaptic calcium regulation in hair cells of the chicken basilar papilla. J Neurosci 34:16688–16697.

Johnson SL, Marcotti W (2008) Biophysical properties of CaV1.3 calcium channels in gerbil inner hair cells. J Physiol 586:1029–1042.

Kennedy HJ (2002) Intracellular calcium regulation in inner hair cells from neonatal mice. Cell Calcium 31:127–136.

Knirsch M, Brandt N, Braig C, Kuhn S, Hirt B, Münkner S, Knipper M, Engel J (2007) Persistence of Ca(v)1.3 Ca2+ channels in mature outer hair cells supports outer hair cell afferent signaling. J Neurosci 27:6442–6451.

Kozel PJ, Friedman RA, Erway LC, Yamoah EN, Liu LH, Riddle T, Duffy JJ, Doetschman T, Miller ML, Cardell EL, Shull GE (1998) Balance and hearing deficits in mice with a null mutation in the gene encoding plasma membrane Ca2+-ATPase isoform 2. J Biol Chem 273:18693–18696.

Kujawa SG, Liberman MC (1999) Long-term sound conditioning enhances cochlear sensitivity. J Neurophysiol 82:863–873.
Lanner JT, Georgiou DK, Joshi AD, Hamilton SL (2010) Ryanodine receptors: structure, expression, molecular details, and function in calcium release. Cold Spring Harb Perspect Biol 2:a003996.
Lelli A, Perin P, Martini M, Ciubotaru CD, Prigioni I, Valli P, Rossi ML, Mammano F (2003) Presynaptic calcium stores modulate afferent release in vestibular hair cells. J Neurosci 23:6894–6903.
Liberman MC (1988) Physiology of cochlear efferent and afferent neurons: direct comparisons in the same animal. Hear Res 34:179–191.
Liberman MC (1990) Effects of chronic cochlear de-efferentation on auditory-nerve response. Hear Res 49:209–223.
Lioudyno MI, Hiel H, Kong J, Katz E, Waldman E, Parameshwaran-Iyer S, Glowatzki E, Fuchs PA (2004) A "synaptoplasmic cistern" mediates rapid inhibition of cochlear hair cells. J Neurosci 24:11160–11164.
Liu C, Glowatzki E, Fuchs PA (2015) Unmyelinated type II afferent neurons report cochlear damage. Proc Natl Acad Sci USA 112:14723–14727.
McGrew SG, Wolleben C, Siegl P, Inui M, Fleischer S (1989) Positive cooperativity of ryanodine binding to the calcium release channel of sarcoplasmic reticulum from heart and skeletal muscle. Biochemistry 28:1686–1691.
Moglie MJ, Fuchs PA, Elgoyhen AB, Goutman JD (2018) Compartmentalization of antagonistic Ca2+ signals in developing cochlear hair cells. Proc Natl Acad Sci USA 115:E2095–E2104.
Oliver D, Klöcker N, Schuck J, Baukrowitz T, Ruppersberg JP, Fakler B (2000) Gating of Ca2+-activated K+ channels controls fast inhibitory synaptic transmission at auditory outer hair cells. Neuron 26:595–601.
Petersen OH (2002) Calcium signal compartmentalization. Biol Res 35:177–182.
Ranum PT, Goodwin AT, Yoshimura H, Kolbe DL, Walls WD, Koh JY, He DZZ, Smith RJH (2019) Insights into the biology of hearing and deafness revealed by single-cell RNA sequencing. Cell Rep 26:3160–3171.e3.
Robertson D, Gummer M (1985) Physiological and morphological characterization of efferent neurones in the guinea pig cochlea. Hear Res 20:63–77.
Saito K (1980) Fine structure of the sensory epithelium of the guinea pig organ of Corti: afferent and efferent synapses of hair cells. J Ultrasructure Res 71:222–232.
Saito K (1990) Freeze-fracture organization of hair cell synapses in the sensory epithelium of guinea pig organ of Corti. J Electron Microsc Tech 15:173–186.
Sakaguchi N, Henzl MT, Thalmann I, Thalmann R, Schulte BA (1998) Oncomodulin is expressed exclusively by outer hair cells in the organ of Corti. J Histochem Cytochem 46:29–39.
Smith CA, Sjöstrand FS (1961) Structure of the nerve endings on the external hair cells of the guinea pig cochlea as studied by serial sections. J Ultrasructure Res 5:523–556.
Sridhar TS, Brown MC, Sewell WF (1997) Unique postsynaptic signaling at the hair cell efferent synapse permits calcium to evoke changes on two time scales. J Neurosci 17:428–437.
Street VA, McKee-Johnson JW, Fonseca RC, Tempel BL, Noben-Trauth K (1998) Mutations in a plasma membrane Ca^{2+}-atpase gene cause deafness in deafwaddler mice. Nat Genet 19:390–394.
Tong B, Hornak AJ, Maison SF, Ohlemiller KK, Liberman MC, Simmons DD (2016) Oncomodulin, an EF-hand Ca^{2+} buffer, is critical for maintaining cochlear function in mice. J Neurosci 36:1631–1635.
Vattino LG, Wedemeyer C, Elgoyhen AB, Katz E (2020) Functional postnatal maturation of the medial olivocochlear efferent – outer hair cell synapse. J Neurosci 40:4842–4857.
Warr WB (1992) Organization of the olivocochlear efferent system in mammals. In: The mammalian auditory pathway: neuroanatomy. (Webster DB, Popper AN, Fay RR, eds). New York: Springer.
Weisstaub N, Vetter DE, Elgoyhen AB, Katz E (2002) The $\alpha 9\alpha 10$ nicotinic acetylcholine receptor is permeable to and is modulated by divalent cations. Hear Res 167:122–135.
Weisz CJC, Glowatzki E, Fuchs PA (2009) The postsynaptic function of type II cochlear afferents. Nature 461:1126–1129.
Weisz CJC, Williams SS-P, Eckard CSC, Divito CBC, Ferreira DDW, Fantetti KNK, Dettwyler SSA, Cai HMH, Rubio ME, Kandler K, Seal RP (2021) Outer hair cell glutamate signaling through type II spiral ganglion afferents activates neurons in the cochlear nucleus in response to non-damaging sounds. J Neurosci 41:2930–2943.
Wong AB, Jing Z, Rutherford MA, Frank T, Strenzke N, Moser T, Rutherford MA, Frank T, Strenzke N, Moser T (2013) Concurrent maturation of inner hair cell synaptic Ca2+ influx and auditory nerve spontaneous activity around hearing onset in mice. J Neurosci 33:10661–10666.
Yamoah EN, Lumpkin EA, Dumont RA, Smith PJS, Hudspeth AJ, Gillespie PG (1998) Plasma membrane Ca2+-ATPase extrudes Ca2+ from hair cell stereocilia. J Neurosci 18:610–624.
Zachary S, Nowak N, Vyas P, Bonanni L, Fuchs PA (2018) Voltage-gated calcium influx modifies cholinergic inhibition of inner hair cells in the immature rat cochlea. J Neurosci 38:5677–5687.
Zhang Y, Glowatzki E, Roux I, Fuchs PA (2020) Nicotine evoked efferent transmitter release onto immature cochlear inner hair cells. J Neurophysiol 124:1377–1387.